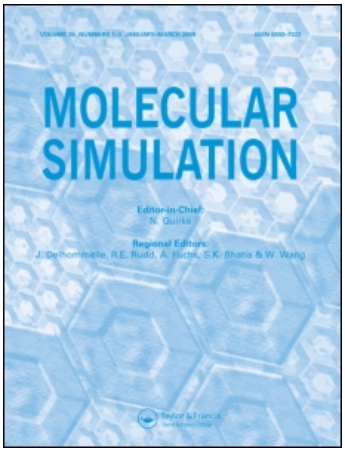

Molecular Simulation
Publication details, including instructions for authors and subscription information:
http://www.informaworld.com/smpp/title~content=t713644482

A Monte Carlo Simulation Study of Orientational Domain Clusters in the Planar Quadrupole Model

M. P. Allen[a]; S. F. O'shea[b]
[a] H.H. Wills Physics Laboratory, Bristol, UK [b] Department of Chemistry, University of Lethbridge, Alberta, Canada

To cite this Article Allen, M. P. and O'shea, S. F.(1987) 'A Monte Carlo Simulation Study of Orientational Domain Clusters in the Planar Quadrupole Model', Molecular Simulation, 1: 1, 47 — 66
To link to this Article: DOI: 10.1080/08927028708080930
URL: http://dx.doi.org/10.1080/08927028708080930

Molecular Simulation, 1987, Vol. 1, pp. 47–66
Photocopying permitted by license only

A MONTE CARLO SIMULATION STUDY OF ORIENTATIONAL DOMAIN CLUSTERS IN THE PLANAR QUADRUPOLE MODEL

M.P. ALLEN*

H.H. Wills Physics Laboratory, Royal Fort, Tyndall Avenue, Bristol BS8 1TL, UK

and

S.F. O'SHEA

Department of Chemistry, University of Lethbridge, Lethbridge, Alberta, Canada T1K 3M4

(*Received October 1986; in final form May 1987*)

We have carried out a series of Monte Carlo simulations of the planar quadrupole model, using the Distributed Array Processor. A very large system size, 16384 molecules, was employed, and special attention was given to orientational domain clustering near the order–disorder transition. Very slow fluctuations of the orientational order parameter, possibly associated with switching from one orientational domain to another, are observed. Close to the phase transition, domain clusters become extremely ramified, with highly irregular borders. On heating through the transition, the low-temperature dominant domain disappears, essentially by becoming a fractal object. The associated Hausdorff dimension decreases from $D = 2$ to $D = 1.6$ as this occurs. Although our results are consistent with a continuous, rather than a first-order, phase transition, effects of finite system size and long time scales prevent us from drawing a definite conclusion on this point.

KEY WORDS: Monte Carlo, phase transitions, orientational order, fractals.

1. INTRODUCTION

In this paper we describe computer simulations of an idealized model for an adsorbed molecular monolayer on a flat solid substrate. This model mimics a variety of physical systems, but the one that invites closest comparison is that of nitrogen molecules adsorbed on graphite. At low temperatures, nitrogen forms a two-dimensional triangular lattice in registry with the graphite basal planes, in a $\sqrt{3} \times \sqrt{3}$ arrangement [1]. The orientations of the molecules are believed to be ordered in a herring-bone structure at low temperature [2], but when the temperature is raised, before the lattice melts, an orientational order–disorder transition occurs [2, 3]. Monte Carlo simulations, using a nearest-neighbour quadrupole–quadrupole interaction, have shown that this simple model exhibits behaviour similar to that of the real system [4]. These preliminary studies used small systems of 36 and 144 molecules. More extensive simulations, employing an approximation to the true quadrupolar interaction, and using system sizes from 400 to 10000, seem to indicate that the order–disorder

*To whom correspondence should be sent.

transition is first order [5] but with large fluctuations. These simulations employed 500–5000 Monte Carlo "sweeps" (attempted moves per molecule) at each temperature. Rather longer runs, up to 22 000 sweeps, have been carried out on systems of 1000 quadrupoles [6]: consistency with the first-order picture was obtained, but the principal aim of the study was to examine the effects of modified boundary conditions.

Here we report the results of much more extensive simulations of the planar quadrupolar system, with a system size of 16 384 molecules and runs of over 50 000 sweeps at temperatures near the phase transition. In part, the aim of this work has been to re-examine the evidence for first-order behaviour. The current wisdom on phase transitions is that first-order transitions cannot be observed in finite-sized systems, such as those used in computer simulation studies. A conventional first-order transition occurs in a catastrophic manner, with the system passing precipitously and irreversibly from one phase to another. No transition precursors are seen. Small-system effects cause rounding of this characteristically discontinuous behaviour, but sharper variation of thermodynamic parameters around the transition will be expected as the system size increases. Continuous transitions, by contrast, are driven by fluctuations, which grow in amplitude and duration on approaching the transition point. The transition is heralded by a diverging correlation length of some kind in the disordered phase. These gross features are expected to become more pronounced on increasing the system size.

The system under study here is closely related to the one studied by Mouritsen and Berlinsky [5], differing from it only in having in the Hamiltonian a scalar term, which was dropped by them as unimportant. The focus of their study was the order of the transition, which is believed to be first order but of a class known as fluctuation-induced. This type of transition is one that appears in mean-field theory as second order but, when the effects of instantaneous fluctuations are included, it is seen to be first order. The transition is thought to occur when the correlation length reaches a finite limiting value, rather than when it diverges. The fluctuations in question are those in the order parameter, and these arise from fluctuations in the structure.

Our principal concern is to study the structural fluctuations observed in a large-scale simulation, and to characterize them quantitatively, if possible. If the transition appears to be truly first order in this case, then first-order transitions in more conventional systems should be readily observable. If, on the other hand, significant high-order-like clustering is observed, we should be able to characterize the clusters quite well in view of the large system size and "long" sampling. With that in mind, we have studied the size distribution of clusters and used fractal analysis to investigate their shapes. The clusters in question are the orientational domains, in other words, the structural fluctuations, near the thermal transition point. Fractal analysis is more commonly associated with higher order transitions, but we are using it here to determine the extent to which (relatively) large, but finite, systems that may be undergoing a first-order phase transition show higher order characteristics.

In section 2, we describe the general simulation strategy, relegating the technical details to the Appendix. In section 3, the thermodynamic results and order parameters observed near the phase transition are given, while section 4 is devoted to the orientational domain analysis. A summary and conclusions appear in section 5.

2. MODEL AND SIMULATION DETAILS

Monte Carlo simulations were carried out on the Queen Mary College Distributed

Array Processor (DAP). A system of 16384 molecules, arranged in a 128 × 128 rhombus with periodic boundary conditions, was employed. The molecular centres were fixed on a regular triangular lattice with lattice spacing R, and molecular orientations were allowed to vary continuously. The molecules were treated as linear, confined to the plane of the lattice, with nearest-neighbour quadrupole–quadrupole interactions as defined in the Appendix. The quadrupole moment θ defines an energy parameter

$$\Gamma = 6\theta^2/25R^5. \quad (1)$$

Both R and Γ are chosen to be unity in the simulations. Previous Monte Carlo simulations [4–6] have shown that this system forms a herring-bone structure of parallel zig-zag chains of molecules, at low temperature, but undergoes an order–disorder transition at $k_BT/\Gamma \approx 11$ where T is the temperature and k_B is Boltzmann's constant. The simulations reported here were concentrated in the region around this phase transition.

The Monte Carlo simulations employed the standard Metropolis method [7]. The nearest-neighbour form of interaction made it possible to consider 4096 independent trial Monte Carlo moves in parallel on the DAP. This was achieved by using four interleaved sublattices of molecules, in a way described in the Appendix. The trial rotation angles were selected randomly from a uniform distribution; the range of possible angles was adjusted continually throughout the simulations, to give an overall acceptance ratio of roughly 50%.

In this work we measure the progress of the simulation in "sweeps", each sweep consisting of 16384 attempted rotational moves, one per molecule. A typical run consists of 8000 sweeps or roughly 1.31×10^8 attempted moves, and takes less than 50 minutes of DAP cpu time. This move rate is, of course, much less than that achievable for Ising lattices [8] because of the need for floating point calculations, but

Table 1 Heating curve.

T	*Sweeps/1000*	u	h
9.00	8	−15.880	0.846
10.80	24	−13.573	0.649
10.90	8	−13.390	0.621
10.95	24	−13.302	0.597
11.00	8	−13.076	0.453
11.05	40	−12.974	0.372
11.10	56	−12.844	0.302
11.15	16	−12.686	0.142
11.20	40	−12.601	0.119
11.25	8	−12.534	0.121
11.30	8	−12.484	0.122
11.35	8	−12.393	0.104
11.40	8	−12.323	0.045
11.50	8	−12.199	0.061
11.55	8	−12.135	0.077
11.60	8	−12.067	0.066
11.65	8	−11.995	0.054
11.70	16	−11.941	0.070
100.00	8	4.190	0.000

T is the temperature, u the configurational energy and h the herring-bone order parameter. We take the energy parameter $\Gamma = 1$. (see Equation (1)).

Table 2 Cooling curve.

T	*Sweeps/1000*	u	h
11.00	16	−13.100	0.472
11.05	32	−12.941	0.350
11.10	40	−12.833	0.266
11.15	8	−12.780	0.305
11.20	8	−12.670	0.206
11.30	8	−12.479	0.144
11.40	24	−12.327	0.117

Symbols as in Table 1.

compares very favourably with quadrupole simulations carried out on scalar computers (see Appendix). A total of 83 runs, each consisting of 8000 sweeps, was carried out. Runs at a particular temperature were initiated from an equilibrated configuration at a neighbouring temperature. Following such a change in state point, one complete run at the new temperature was allocated for equilibration, and a subsequent one or more runs used to produce simulation averages. Most effort was concentrated close to the transition temperature itself.

The simulations were organized into two independent sequences. The starting point for the heating sequence was the perfect herring-bone lattice, and changes in state point always consisted of raising the temperature. The total number of production run sweeps carried out at each state point in this sequence is reported in Table 1. The starting point for the cooling sequence was a configuration of random orientations, and the temperature was progressively lowered from one state point to the next. Total run lengths for this sequence are given in Table 2. In each case, thermodynamic quantities and orientational order parameters were calculated, and these are discussed in section 3. For 11 of the runs, additional analysis was performed. In these cases, complete configurations were written to magnetic tape at intervals of 10 sweeps. Analysis of the clustering behaviour and fractal characteristics for these runs is given in section 4.

3. THERMODYNAMICS AND ORDER PARAMETERS

The simulation average of the configurational energy per particle

$$u = \frac{1}{N} \sum_{\{i,j\}} u_{ij} \tag{2}$$

is reported for each temperature in Tables 1 and 2. The results close to the phase transition are plotted in Figure 1. In the graph we subtract the classical harmonic lattice contribution to the configurational energy, i.e. we plot

$$u' = u - u_0 - \tfrac{1}{2} k_B T \tag{3}$$

with $u_0 = -21.484375\Gamma$ here, in order to reduce the variation with temperature. The statistical precision of these results is estimated by analyzing block-averages as described in the Appendix. A smooth curve, having the form of a hyperbolic tangent superimposed on a polynomial function of T, was fitted through the data points (see Appendix). The excess heat capacity, obtained as the temperature derivative of the

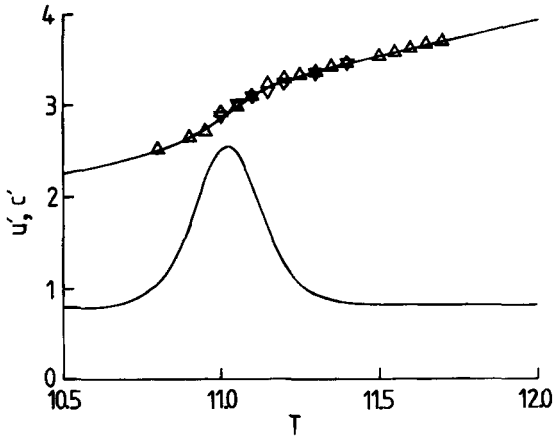

Figure 1 The configurational (excess) energy u', with the classical harmonic lattice contribution subtracted, vs temperature. Up triangles correspond to heating sequences and down triangles to cooling sequences. The error bars are smaller than the plotting symbols. The curves are a least-squares fit discussed in the Appendix and the corresponding excess heat capacity obtained from the temperature derivative.

fit to u', is also shown in Figure 1. It has a peak at $k_BT \approx 11.03$. Values of the heat capacity calculated from the configurational energy fluctuations are consistent with this curve within their (significant) statistical errors. No discontinuous jumps in u' and no hysteresis effects are seen.

A more sensitive quantity is the orientational order parameter. In our system there are three equivalent herring-bone order parameters, corresponding to the three possible zero-temperature structures [5]. These may be written

$$h_\alpha = \frac{1}{N}\left\langle \sum_i \sin(2\phi_i - 2\theta_\alpha) \exp(i\boldsymbol{k}_\alpha \cdot \boldsymbol{R}_i) \right\rangle, \alpha = 1, 2, 3$$

$$= \frac{1}{N}\left\langle \sum_i \sin(2\phi_i - 2\theta_\alpha)(-1)^{K_{i\alpha}} \right\rangle, \alpha = 1, 2, 3, \tag{4}$$

where $\boldsymbol{k}_\alpha$ is a wave-vector chosen to give alternating signs $\exp(i\boldsymbol{k}_\alpha \cdot \boldsymbol{R}_i) = (-1)^{K_{i\alpha}}$ for successive rows of molecules. The directions of these rows are determined by the value of α: θ_α is the angle of rows with respect to a reference direction and $\boldsymbol{k}_\alpha$ is perpendicular to the rows. Specifically

$$\begin{aligned} \theta_1 &= 0 & \boldsymbol{k}_1 &= \frac{\pi}{R}(0, 2/\sqrt{3}) \\ \theta_2 &= \pi/3 & \boldsymbol{k}_2 &= \frac{\pi}{R}(-1, 1/\sqrt{3}) \\ \theta_3 &= 2\pi/3 & \boldsymbol{k}_3 &= \frac{\pi}{R}(-1, -1/\sqrt{3}). \end{aligned} \tag{5}$$

The h_α parameters lie between -1 and 1. Below the phase transition, one herring-bone structure dominates and a high absolute value of the corresponding h_α occurs, the other components being small. Above the phase transition, all three domains are

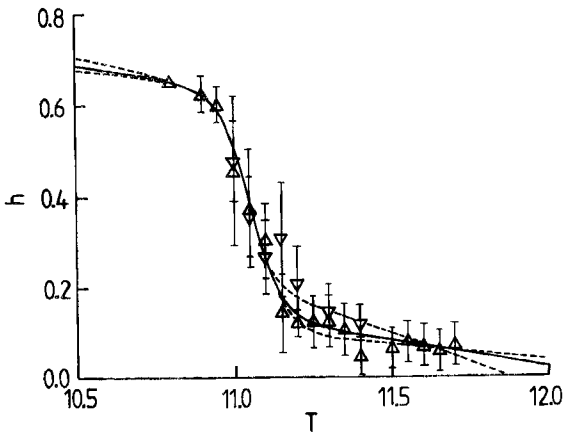

Figure 2 The herring-bone order parameter h vs temperature. Notation as for Figure 1. The error bars are of length $2\sigma(\tau_{run})$ as defined in Equation (A7). Dashed lines are fits to heating and cooling data only in the transition region.

found in equal amounts, forming small clusters, and all three h_αs fluctuate about zero. In Tables 1 and 2 we report the values of

$$h = \max(|\langle h_1 \rangle|, |\langle h_2 \rangle|, |\langle h_3 \rangle|). \quad (6)$$

The behaviour around the phase transition is shown in Figure 2. Again, the error analysis is described in the Appendix. As can be seen, a smooth variation of h occurs with a change from the high values characterizing the ordered phase to the small positive values of the disordered phase taking place at $k_B T/\Gamma \approx 11.05$. The order parameter data was fitted using the same tanh function curve superimposed on a polynomial in T, and this is illustrated in Figure 2. To check for hysteresis, separate fits were made to the heating and cooling data, and these are also shown in the figure. More specifically, values outside the transition range $11.00 \leqslant T \leqslant 11.40$ were assumed to be independent of hysteresis effects, and the Table 1 values were used for both the additional fits; however, the heating curve values within the transition range were taken from Table 1, while the cooling curve values were taken from Table 2. No evidence for a hysteresis loop can be seen. At temperatures just above the transition ($T \approx 11.05$), the cooling curve lies slightly above the corresponding heating curve, which is the reverse of what would be expected should hysteresis occur.

Our data also do not allow us to infer the presence of a discontinuous change in h, and there was no tendency in the fitting process for the "width" of the tanh function to decrease to zero giving a step discontinuity. No forbidden range of h values seems to exist. However, the error bars on h at the temperatures $T = 11.05$ and $T = 11.10$ are quite significant, and result from very slow fluctuations of the order parameters near the transition (see below). A quantitative measure of this is provided by the "statistical inefficiency", or the correlation "time" (in MC sweeps) of the order parameters, as discussed in the Appendix. Away from the phase transition, values of order 1000 sweeps are typical, but at $T = 11.05$ and $T = 11.10$ values of at least 10 000 sweeps seem to be indicated.

The parameter h is not a unique measure of ordering, of course. In particular, since each h_α may fluctuate slowly near the phase transition, taking on positive and negative

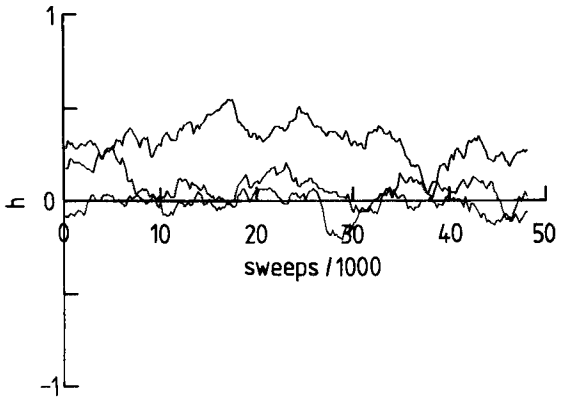

Figure 3 Variation of block averages of the three order parameters h_α during a run at $k_B T/\Gamma = 11.10$.

values, the definition above, which takes the moduli of simulation averages, may yield slightly different results in different simulation runs. Indeed, for runs of infinite length, h should vanish. Even in the ordered phase, one might expect the system to sample each of the three ordered structures, with equal likelihood of positive and negative contributions to h, given sufficient simulation time. To test whether this affects our results, we also calculated the order parameters

$$h' = \max(\langle|h_1|\rangle, \langle|h_2|\rangle, \langle|h_3|\rangle) \tag{7}$$

and

$$h'' = (\langle h_1^2 + h_2^2 + h_3^2\rangle)^{1/2} \tag{8}$$

for some of the runs near the transition point. Only minor quantitative differences from the h results were seen. The slow variation of the h_α with simulation "time", measured as a sequence of block averages over 200 sweeps, is illustrated in Figure 3. This type of behaviour has been noted before in simulations of the quadrupolar system [6] and of quadrupolar bilayers [9].

4. ORIENTATIONAL DOMAINS AND FRACTAL ANALYSIS

For each of 11 selected simulation runs, sets of 800 configurations were analyzed to determine features of the orientational domain structure.

The method used to identify herring-bone domains is straightforward, and essentially dictated by our desire to assign each molecule on the lattice to one, and only one, of the three herring-bone orientations. The glide symmetry lines of the three domains are oriented at angles of 0, $2\pi/3$ and $4\pi/3$ (say) relative to a coordinate system fixed in the lattice. In perfect (zero temperature) domains, four molecular orientations occur, at $\pi/4$, $3\pi/4$, $5\pi/4$ and $7\pi/4$ relative to the glide lines (but this amounts to two equivalent pairs since the molecules have two-fold rotational symmetry). Thus, a unit vector lying along the axis of a molecule chosen from any of the perfect herring-bone domains will point in one of 12 equivalent, equally-spaced directions in the range $(0, 2\pi)$. At non-zero temperatures, fluctuations around the perfect lattice directions will occur. To assign each molecule in a configuration to a domain, orientation space is

divided into 12 equal regions, each with a perfect lattice direction at the centre. Whichever orientational "bin" the molecule lies in serves to define which of the three domains it belongs to. The bin width, $\pi/6$, is the largest possible consistent with the requirement that each molecule shall be assigned to only one domain; this choice ensures that no molecules are excluded and it allows significant deviations from the perfect lattice orientations.

Contiguous domains of molecules belonging to the same herring-bone arrangement were then identified by a parallel clustering algorithm. This algorithm, called the "ants-in-a-labyrinth" method, has been developed independently [10] in connection with the two-dimensional percolation problem. It is described in the Appendix. Having identified the clusters, geometrical quantities characterizing their size and shape can be calculated, and we turn to this below. However, visual inspection of "snapshot" configurations, with the three herring-bone patterns picked out in different colours (red, blue and green) is also very revealing. Figure 4(a) shows a typical configuration close to the phase transition, at $k_B T/\Gamma = 11.05$. To make the cluster boundaries more obvious, a coarse-graining approach is used. At each site a majority rule is applied: if a clear majority of the six neighbouring molecules plus the molecule at that site belong to a single herring-bone structure, then the site is marked accordingly; if no clear majority exists, the site is left blank. Figure 4(b) is based on the same configuration as Figure 4(a), and clearly shows a ramified orientational structure. Figure 4(c) is taken from a run well below the transition, at $k_B T/\Gamma = 10.80$, and Figure 4(d) from a run well above the transition, at $k_B T/\Gamma = 11.30$. We shall refer to these snapshots in the quantitative analysis of cluster sizes and shapes which follows. We emphasize that coarse-graining is used for visual clarity only and is not employed in the analysis.

The simplest cluster property is the size or area A, i.e. the total number of molecules comprising it. In Table 3, we give the distribution of cluster sizes for each of the eleven selected runs. We choose to break down the size range into "octaves": bins whose "width" doubles from one to the next. The lowest bins ($A < 64$) are all grouped together. For each bin, we report the fraction of the total area (16 384 units per configuration) covered by clusters in the corresponding size range. At low temperatures, this distribution is doubly peaked, with a large fraction of the area covered by a single large domain, and the remainder consisting of many very small clusters. Very few clusters in the range 65–4096 are seen. This picture is borne out by Figure 4(c): the herring-bone order parameter measured in the simulations is essentially dictated by the area covered by the background cluster. At high temperatures there are also very few moderate sized clusters, and no large ones at all. Figure 4(d) confirms the existence of small clusters, with an orientational correlation length of a few lattice spacings. There is no preferred "background".

Close to the transition, a different pattern is seen. Slightly more than half of the area is covered by clusters of size 64 or less. The remaining area is occupied by clusters of all sizes up to the largest compatible with the system size. The precise distribution varies somewhat, but a striking feature of the results is the relative constancy of the percentage coverage of each size range, at a value of 4–8%, for each case. Bearing in mind the changing bin size, this means that an area A is almost equally likely to be covered by a single contiguous cluster of size A, two clusters each of size $A/2$, four of size $A/4$, or any other suitable combination of clusters of different sizes. This seems to be consistent with the association of the transition with slow critical-like fluctuations of large length scale, prominent domain walls, and continual transformation

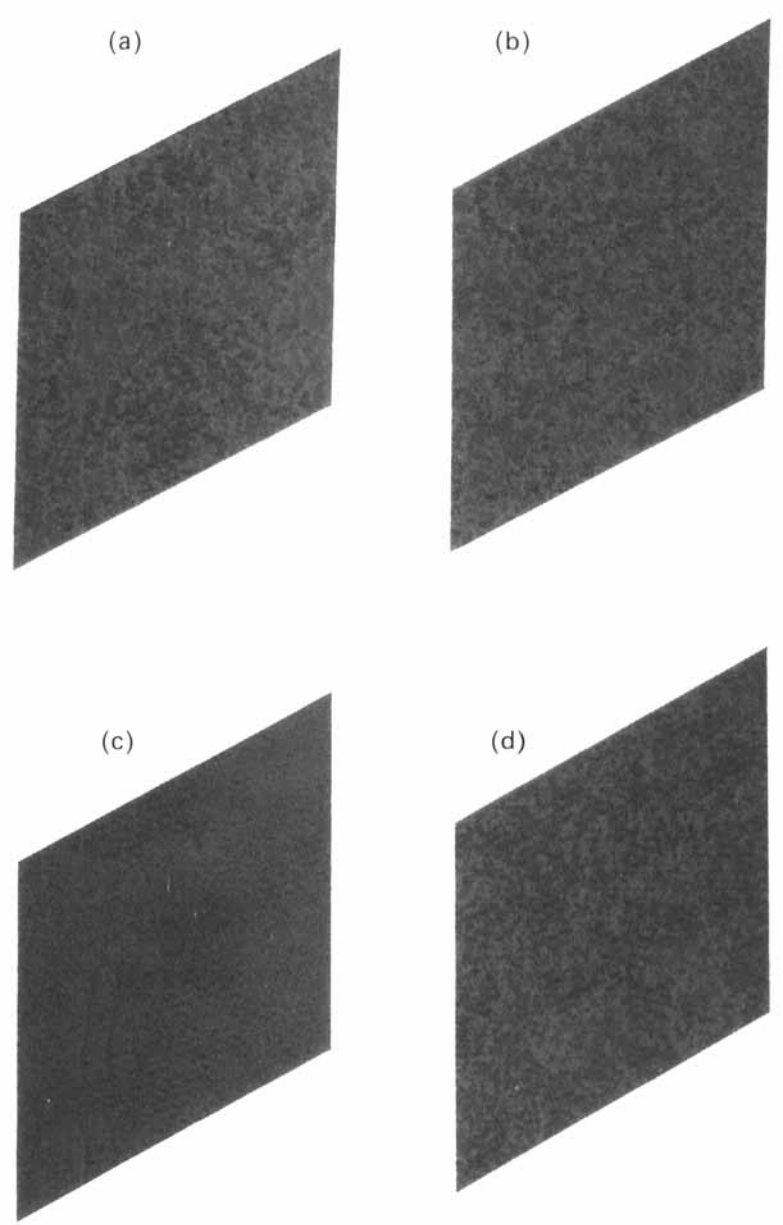

Figure 4 Typical configurations. Each molecule is represented by a line segment. Different orientational domains are represented by different colours. (a) Near the phase transition, $k_B T/\Gamma = 11.05$; (b) the same configuration using coarse graining; (c) a low-temperature configuration $k_B T/\Gamma = 10.80$ using coarse graining; (d) a high-temperature configuration $k_B T/\Gamma = 11.30$ using coarse graining. (See colour plates I–IV.)

Table 3 Orientational domains.

Run	*A*	*B*	*C*	*D*	*E*	*F*	*G*	*H*	*I*	*J*	*K*
T	9.00	10.80	11.00	11.00	11.05	11.05	11.05	11.05	11.10	11.70	100.0
Bin size	*h*	*h*	*c*	*c*	*h*	*h*	*c*	*c*	*c*	*h*	*h*
a 1–64	32.8	51.2	58.8	60.4	61.4	62.9	61.9	60.4	64.3	76.2	98.7
b 65–128	0.0	1.7	5.0	6.4	6.9	7.8	6.9	6.0	8.4	11.4	1.3
c 129–256	0.0	0.9	4.7	6.7	7.0	7.9	7.1	5.4	8.5	8.3	0.0
d 257–512	0.0	0.3	4.5	6.5	6.8	8.3	7.3	5.3	8.4	3.5	0.0
e 513–1024	0.0	0.2	4.4	3.8	6.0	6.9	7.9	4.9	7.1	0.6	0.0
f 1025–2048	0.0	0.0	4.3	3.7	7.0	4.6	6.2	4.9	3.2	0.0	0.0
g 2049–4096	0.0	0.0	8.8	11.4	4.9	1.6	2.8	9.4	0.1	0.0	0.0
h 4097–8192	0.0	44.3	9.4	1.1	0.0	0.0	0.0	3.7	0.0	0.0	0.0
i 8193–16384	67.2	1.3	0.0	0.0	0.0	0.0	0.0	0.0	0.0	0.0	0.0
D	2.0	1.9	1.7	1.7	1.6	1.6	1.6	1.7	1.6	–	–

The first part of the table identifies the run, with *h* and *c* denoting heating and cooling branch respectively. The runs are labelled with upper case letters. The second part gives the percentage of the total area covered by clusters of sizes lying in the range appearing in the leftmost column. The size bins are identified by lower case letters. The last part gives an estimate of the fractal dimension *D* of the larger clusters (averaged over bins *f*–*i*).

between one herring-bone domain and another [6, 9]. Close to the phase transition, the cluster boundaries become highly irregular, and the clusters themselves are riddled with "holes" (i.e. smaller clusters of different herring-bone structures). This can be seen in Figure 4(b), which clearly shows structures of all length scales below that of the simulation box. Despite the obvious complexity of the orientational domain structures, it is notable that, below the phase transition, it is always possible to identify a single cluster, albeit a very ramified one, spanning the entire system. Above the phase transition, no such cluster exists. Thus, the situation is very analogous to that of percolation.

In these clusters, almost all the molecules are on the boundary. It thus becomes meaningless to measure shape parameters such as A/L^2 where L is the boundary

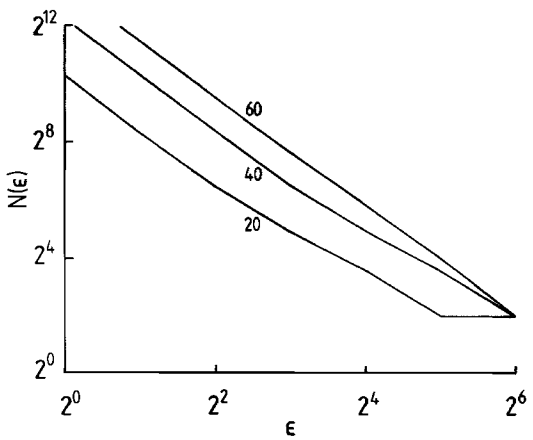

Figure 5 Fractal analysis of the areas of test clusters. We plot $\log_2 N$, where N is the number of rhomboidal cells traversed by the cluster pattern, vs $\log_2 \varepsilon$, where ε is the length of the cell side. The curves correspond to discs of radius 20, 40, and 60 lattice spacings as indicated.

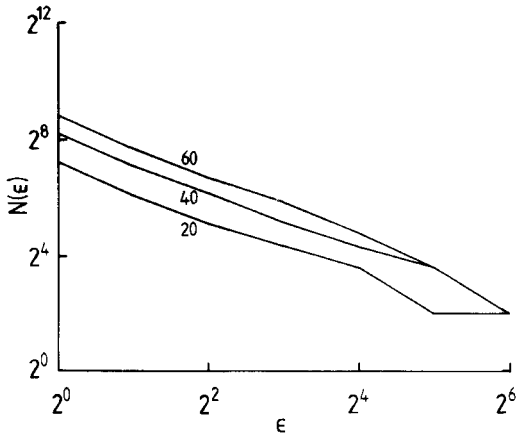

Figure 6 Fractal analysis of the boundaries of test clusters. Notation as for Figure 5.

length and A the area. A more fundamental analysis based on fractal dimension is needed [11]. We have written a program to determine the Hausdorff dimension D of clusters in a parallel fashion on the DAP. An operational definition of this quantity is as follows. The rhomboidal simulation box is covered by a tesselation of rhomboidal cells with sides of length ε, which may take values from one lattice spacing up to the complete box length, rising in powers of two. For each choice of ε, a count is made of the number of rhomboidal cells containing some of the cluster pattern. For a two-dimensional entity (i.e. a cluster with smooth boundaries and no holes) this number $N(\varepsilon)$ should decrease as ε^{-2}; for a one-dimensional entity (e.g. the boundary of such a cluster) it will vary as ε^{-1}; and in general it will vary as ε^{-D}. Once again, the details of the algorithm appear in the Appendix. It was tested on artificial "clusters" consisting of nearly circular discs of molecules of one orientation embedded in a background of a different orientation. Discs of radius 20, 40 and 60 lattice spacings

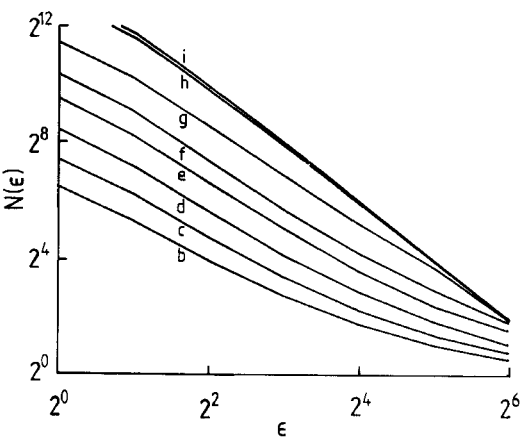

Figure 7 Fractal analysis for run B, $k_BT/\Gamma = 10.80$, below the phase transition. Plotted curves are averages over all clusters falling within the size range defined by the labels. The cluster size increases from b to i (see Table 3). Otherwise notation as for Figure 5.

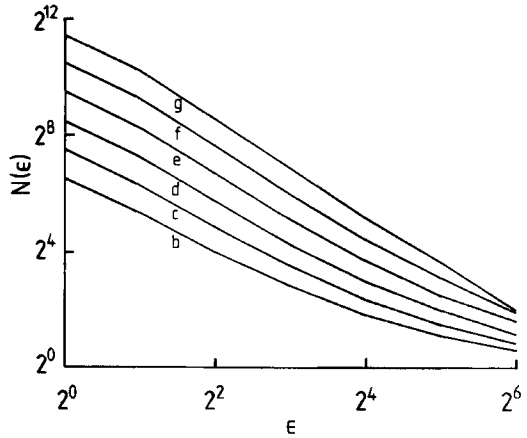

Figure 8 Fractal analysis for run E, $k_BT/\Gamma = 11.05$, close to the phase transition. Notation as for Figure 7.

were used. Log_2–$\log_2$ plots of $N(\varepsilon)$ vs ε are shown in Figure 5, and they show the expected linear form with gradient $= -2$. Deviations from linearity are seen when ε approaches the disc size. Similar plots are shown in Figure 6 for the patterns consisting of the boundaries of the discs (i.e. those sites not surrounded by others of the same orientation). As expected, linear plots with gradient $= -1$ are seen. The method was also hand-checked by drawing shapes on graph paper and counting squares.

Each configuration saved from the 11 runs of Table 3 was analyzed, the above procedure being applied to every cluster of size $A > 64$. The curves of $N(\varepsilon)$ were averaged over all clusters, and were also divided into the size bins of Table 3 and averaged over the clusters falling in each bin. This gives a useful check on finite size effects for the smaller clusters. Typical results are shown in Figures 7–9. Well below the phase transition, at $k_BT/\Gamma = 10.80$ (Figure 7) the larger clusters give straight line plots of $\log_2 N(\varepsilon)$ vs $\log_2 \varepsilon$ with gradient -2 over a substantial range of ε,

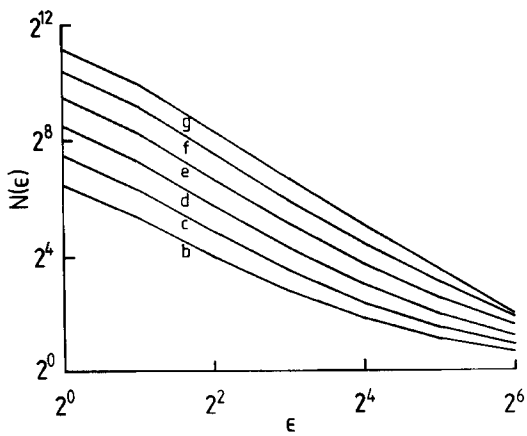

Figure 9 Fractal analysis for run I, $k_BT/\Gamma = 11.10$, above the phase transition. Notation as for Figure 7.

corresponding to few holes and smooth boundaries. The smaller clusters tend to give curved plots with lower gradients, and the effects of finite cluster size can be seen as ε increases. Most of the curves in Figure 7 correspond to averages over very few clusters in the medium-size range, less than 0.1% of the total in some cases (see Table 3). Very close to the transition, however, the gradient decreases in magnitude even for the larger clusters, while self-similarity still seems to be indicated by the linearity of the plots. At $k_B T/\Gamma = 11.05$ the apparent fractal dimension of the clusters is $D \approx 1.6$ (see Figure 8). Above the transition, at $k_B T/\Gamma = 11.10$ (Figure 9), the largest clusters are of area $A \approx 3000$, still large enough to give a significant linear plot. Above this temperature, statistics on the larger clusters becomes poor.

In Table 3 we summarize our estimates for the fractal dimension of clusters, taking area-weighted averages of the gradients of the curves of $\log_2 N(\varepsilon)$ vs $\log_2 \varepsilon$ to define D and restricting our interest to clusters with $A > 1024$ (bins *f–i*) to eliminate effects of small size.

5. DISCUSSION

We have carried out an investigation of the planar quadrupole model, for a very large system size, by Monte Carlo simulation on the DAP. We have concentrated on the region close to the orientational order–disorder transition in this system, with special attention given to the domain cluster properties.

The evidence to date [4, 5, 6] suggests that the transition is first-order, but we are principally interested in the characteristics of the transition that reflect higher order attributes. Our thermodynamic and order-parameter results are consistent with a continuous transition at $k_B T/\Gamma \approx 11.05$, but these cannot be viewed as conclusive evidence, either way, since they are expected to exhibit finite-size effects even in the conventional first-order case (for an example, see [12]). It may also be that the "scalar part" of the interaction, included here but omitted as irrelevant by Mouritsen and Berlinsky [5], may mask some of the first-order character and make it more difficult to detect.

The variation of order parameters near the phase transition in our work does not seem to agree with the results of Evans *et al.* [6]: here we can only point out that our simulations were rather longer, and at more closely-spaced temperatures, than those of Reference [6], as well as being for a system more than 16 times larger. None of these factors, however, alleviates the problem of slow switching between one orientational domain and another in the vicinity of the phase transition, which was reported in the previous work [6] and is certainly a feature of our own. An examination of the system-size dependence was an essential feature of the work of Mouritsen and Berlinsky [5], and would be helpful here. Our specific heat peak seems to be rather narrower, but of approximately the same height, as that of Reference [6]; a quantitative comparison does not seem fruitful, however, since the latter authors employed a very elongated simulation box. There seems to be virtually no system-size dependence of the energy or heat capacity in the analogous planar rotor system [5] for 400 or more molecules.

We examined the orientational structure of this system in some detail. Close to the phase transition, the orientational domain clusters become extremely ramified, with highly irregular borders. A phenomenon analogous to percolation seems to operate. The distribution of cluster sizes was examined. This indicated that clusters of all

possible sizes appear at the transition. Visual inspection confirmed the disappearance of the low-temperature background cluster on approaching the transition, essentially by a process of its becoming a fractal object rather than by simply diminishing in area.

We analyzed the larger clusters in terms of their apparent fractal dimension, which decreased from $D = 2$ to $D = 1.6$ on heating through the transition. This should be compared with the values for percolation clusters ($D = 1.89$), diffusion-limited aggregates ($D = 1.67$) and lattice animals ($D = 1.56$) [13].

The advantage of the fractal approach is that the initial identification of domains is carried out on the smallest length scale in the system, namely the lattice spacing, and that the consequences of increasing this length scale are then explored in a quantitative fashion.

For a system of finite size, and with a well-defined lower bound to the length scale set by the lattice spacing, it is, of course, difficult to produce convincing evidence for self-similar behaviour. In particular, it may be that part of the variation of D is due to changes in the distribution of cluster sizes, with finite cluster size effects influencing the analysis as the length scale ε increases. We have tried to avoid these difficulties by conducting separate analyses for clusters in the different size ranges, and by restricting our attention to the larger clusters in the final analysis.

The fractal properties of the clusters seen in this study can be set alongside the usual characteristics (long-range correlations, smoothly varying order parameters) of a continuous transition, but they might equally well be expected close to a fluctuation-induced first-order transition of the kind proposed by Mouritsen and Berlinsky. The question of the order of the transition cannot be settled by studies of a single system size, and it is clear that further extension of the work of Reference [5] is desirable.

Acknowledgements

Part of this work was carried out while one of us (S.F.O.) was a visitor at the University Chemical Laboratories, Cambridge, and the other (M.P.A.) held an S.E.R.C. Advanced Fellowship at the Physical Chemistry Laboratory, Oxford. We thank the respective institutions for their hospitality. We have also benefited from conversations with D.J. Tildesley, R.K. Thomas, and members of the DAP Support Unit at Queen Mary College. This research was supported by the Science and Engineering Research Council, and by the National Science and Engineering Research Council of Canada.

References

[1] J.K. Kjems, L. Passell, H. Taub and J.G. Dash, "Neutron scattering from nitrogen adsorbed on basal-plane oriented graphite", *Phys. Rev. Lett.*, **32**, 724 (1974); J.K. Kjems, L. Passell, H. Taub, J.G. Dash and A.D. Novaco, "Neutron scattering study of nitrogen adsorbed on basal-plane-oriented graphite", *Phys. Rev.*, **B13**, 1446 (1976).

[2] R.D. Diehl, M.F. Toney and S.C. Fain, "Orientational ordering of nitrogen molecular axes for a commensurate monolayer physisorbed on graphite", *Phys. Rev. Lett.*, **48**, 177 (1982).

[3] J. Eckert, W.B. Ellerson, J.B. Hastings and L. Passell, "Neutron scattering as a probe of the orientational ordering of nitrogen molecules on graphite", *Phys. Rev. Lett.* **43**, 1329 (1979); A.D. Migone, H.K. Kim, M.H.W. Chan, J. Talbot, D.J. Tildesley and W.A. Steele, "Studies of the orientational ordering transition in nitrogen adsorbed on graphite", *Phys. Rev. Lett.*, **51**, 192 (1983).

[4] S.F. O'Shea and M.L. Klein, "Orientational phases of classical quadrupoles on a triangular net", *Chem. Phys. Lett.*, **66**, 381 (1979).

[5] O.G. Mouritsen and A.J. Berlinsky, "Fluctuation-induced first-order phase transition in an anisotropic planar model of N_2 on graphite", *Phys. Rev. Lett.*, **48**, 181 (1982); O.G. Mouritsen, *Computer Studies of Phase Transitions and Critical Phenomena*, Springer-Verlag, New York, 1984, Section 5.3.
[6] H. Evans, D.J. Tildesley and T.J. Sluckin, "Boundary effects in the orientational ordering of adsorbed nitrogen", *J. Phys.*, **C17**, 4907 (1984).
[7] N. Metropolis, A.W. Rosenbluth, M.N. Rosenbluth, A.H. Teller and E. Teller, "Equation of state calculations by fast computing machines", *J. Chem. Phys.*, **21**, 1087 (1953).
[8] K. Binder, "Recent trends in the development and application of the Monte Carlo method", in *Monte Carlo Methods in Statistical Physics, Topics in Current Physics* **7**, 2nd ed., K. Binder, ed., Springer-Verlag, New York, 1986, Ch. 10.
[9] S.F. O'Shea and M.L. Klein, "Orientational phases of a quadrupolar bilayer", *Phys. Rev.*, **B25**, 5882 (1982).
[10] R. Dewar and C.K. Harris, "Parallel computation of cluster properties: application to 2D percolation", *J. Phys. A*, **20**, 985 (1987).
[11] B. Mandelbrot, *The Fractal Geometry of Nature*, Freeman, Oxford, 1982.
[12] M.S. Challa, D.P. Landau and K. Binder, "Finite-size effects at temperature-driven first-order transitions", *Phys. Rev.* **B34**, 1841 (1986).
[13] R.M. Malzbender, R.C. Mockler and W.J. O'Sullivan, "Topological and geometrical properties of DLA clusters", *J. Phys.* **A18**, L1143 (1985); S. Havlin, Z.V. Djordjevic, I. Majid, H.E. Stanley and G.H. Weiss, "Relation between dynamic transport properties and static topological structure for the lattice animal model of branched polymers", *Phys. Rev. Lett.*, **53**, 178 (1984); T.A. Witten and L.M. Sander, "Diffusion-limited aggregation, a kinetic critical phenomenon", *Phys. Rev. Lett.*, **47**, 1400 (1981).
[14] W. Oed, "Monte Carlo simulation on vector machines", *Ang. Informatik*, **7**, 358 (1982); G.S. Pawley, R.H. Swendsen, D.J. Wallace and K.G. Wilson, "Monte Carlo renormalization group calculations of critical behaviour in the simple-cubic Ising model", *Phys. Rev.*, **B29**, 4030 (1984).
[15] D.J. Tildesley, private communication.
[16] R. Friedberg and J.E. Cameron "Test of the Monte Carlo method: fast simulation of a small Ising lattice", *J. Chem. Phys.*, **52**, 6049 (1970).
[17] G. Jacucci and A. Rahman, "Comparing the efficiency of Metropolis Monte Carlo and molecular dynamics methods for configuration space sampling", *Il Nuovo Cimento*, **D4**, 341 (1984).
[18] D. Fincham, N. Quirke and D.J. Tildesley, "Computer simulation of molecular liquid mixtures. I. A diatomic Lennard-Jones model mixture for CO_2/C_2H_6", *J. Chem. Phys.*, **84**, 4535 (1986).
[19] H. Müller-Krumbhaar and K. Binder, "Dynamic properties of the Monte Carlo method in statistical mechanics", *J. Stat. Phys.*, **8**, 1 (1973).
[20] A. Papoulis, *Probability, Random Variables, and Stochastic Processes*, McGraw-Hill, New York, 1965, Ch. 9.
[21] P.R. Bevington, *Data Reduction and Error Analysis for the Physical Sciences*, McGraw-Hill, New York, 1969.

APPENDIX

Here we summarize technical details of the simulation and methods of data analysis.

The total potential energy of our triangular lattice is defined as a sum of distinct nearest-neighbour pairwise interactions of the following form:

$$U_{ij} = \frac{3\theta^2}{4R^5}\{1 - 5c_i^2 - 5c_j^2 + 35c_i^2c_j^2 + 2c_{ij}^2 - 20c_ic_jc_{ij}\}. \tag{A1}$$

Here, θ is the quadrupole moment, R the lattice spacing, and

$$\begin{aligned} c_i &= \hat{\boldsymbol{e}}_i \cdot \hat{\boldsymbol{R}}_{ij} \\ c_j &= \hat{\boldsymbol{e}}_j \cdot \hat{\boldsymbol{R}}_{ij} \\ c_{ij} &= \hat{\boldsymbol{e}}_i \cdot \hat{\boldsymbol{e}}_j \end{aligned} \tag{A2}$$

where $\hat{e}_i$, $\hat{e}_j$ are unit vectors along the molecular axes and $\hat{R}_{ij}$ is the unit vector pointing from j to i. Simulation units were chosen to make the lattice spacing and the energy parameter

$$\Gamma = 6\theta^2/25R^2 \tag{A3}$$

equal to unity, as in Reference [4]. In other work [6] the quantity $K = 3\theta^2/16R^5$ is taken as a convenient energy unit, while in simulations of the analogous planar spin model [5] a quantity $K = 105\theta^2/32R^5$ is employed.

The simulation technique employed is conventional constant-NVT Metropolis Monte Carlo [7] with single-particle rotational moves chosen to give 50% acceptance rate. The lattice structure of the problem allows a mapping of the 128 × 128 rhombic simulation "box" onto the 64 × 64 DAP processor array. In fact, four interleaved sublattices are considered, the 4096 molecules on each sublattice being represented by a single DAP Fortran matrix variable. Each molecule belonging to a given sublattice has, as its six neighbours, two molecules belonging to each of the other three sublattices. As the interactions are between nearest neighbours only, a completely parallel Monte Carlo algorithm may be constructed, based on this interleaved sublattice structure [14]. Since none of the molecules on a given sublattice interact directly with each other, all of them can be considered simultaneously and independently for Monte Carlo moves. A complete set of trial rotations is generated from a uniform distribution of angles within a restricted range. The ratios of old and new Boltzmann factors for the sublattice of molecules are calculated and compared with random numbers in the usual fashion. In this way, 4096 logical switches are set and used as a mask to accept or reject the moves on the sublattice, and the new orientations are defined accordingly. The instantaneous values of potential energy and order parameters are updated by summing the contributions from each accepted move. The whole procedure is repeated for each sublattice in turn. The complete process of attempting one move for every molecule in the system is referred to as a "sweep". Overall, a rate of 44 000 attempted moves were made per second: for comparison, in the work of Reference [6] roughly 3700 attempted moves per second were achieved on a CDC 7600 [15].

The identification of clusters of given herring-bone structures was also conducted in parallel. The initial assignment of each molecule to a given herring-bone domain, as described in section 4 of the text, is straightforwardly achieved by integerizing the orientation matrix variables. Each of the three herring-bone structures is then tackled separately. The molecules belonging to a specific herring-bone arrangement are stored in a set of four logical matrices (i.e. a set of 128 × 128 "true" or "false" values). The aim is to identify each contiguous cluster of "true" values, and analyze its properties [10]. One of the true values is picked out and the corresponding element of an initially blank ("false") set of matrices set to "true". This is the "ant". "True" values (ant offspring) are then placed at the neighbouring six sites of the triangular lattice, but only where a "true" exists in the original pattern.

This process is repeated iteratively, until no change in the ant population occurs. The algorithm corresponds to the ants spreading from their initial position through the labyrinth mapped out in the original pattern, but stopping at the boundary of the cluster in which the initial position is located. The parallelism stems from the advancement of the ant population frontier as a whole, in a single step. Once a cluster has been identified and analyzed, it is removed from the original pattern and the whole procedure repeated until the pattern is gone. Since our interest lay in the properties

of moderate and large clusters, the efficiency of the method was increased by "burning off" [10] isolated molecules (cluster size 1) before embarking on the full analysis. Further improvement could have resulted from burning off more of the small clusters, but this was thought unnecessary: the total DAP time spent on the cluster analysis was a small fraction of the time involved in the original simulations.

The final area in which the parallel architecture of the DAP was exploited is the calculation of the Hausdorff dimension D for each cluster of interest. The definition of D involves counting the number of rhombi $N(\varepsilon)$ in a tesselation of rhombi of side ε that contain some of the cluster pattern. To begin with, the pattern is stored in four 64×64 logical matrix variables (one for each sublattice). The DAP SUM function is used to give the value of N for $\varepsilon = 1$, in other words the conventional cluster area A. By combining the four logical matrices into one, using the logical OR function, and SUMming the bits, the value $N(\varepsilon = 2)$ is obtained. Subsequent operations are carried out on this one logical matrix. Each point in the pattern is duplicated or "smeared out" over a 2×2 rhombus using the logical SHIFT and OR functions: thus, each "true" bit at position (i, j) generates, at the next stage, "true" bits at (i, j), $(i + 1, j)$, $(i, j + 1)$ and $(i + 1, j + 1)$. A masking matrix, true only where both i and j are even, is used to select those double-sized rhombi in which parts of the cluster appear. All these operations are conducted in parallel, and a SUM gives $N(\varepsilon = 4)$. The procedure is repeated to give $N(\varepsilon = 8)$, $N(\varepsilon = 16)$ etc.

Finally, we turn to the methods used to estimate the statistical imprecision in our simulation averages and to fit the data. To account for serial correlations in the Monte Carlo runs, we analyzed block averages as a function of block length, thus obtaining an estimate of the "statistical inefficiency" [16, 17]. Specifically, suppose that we split the whole simulation run of τ_{run} sweeps at a particular state point into n_b blocks each consisting of τ_b sweeps, so $n_b \tau_b = \tau_{run}$. The mean value of, say, the configurational energy is calculated for each block b and we call this $\langle u \rangle_b$:

$$\langle u \rangle_b = \frac{1}{\tau_b} \sum_{\tau=1}^{\tau_b} u((b-1)\tau_b + \tau). \tag{A4}$$

These block averages are used to calculate a variance

$$\sigma^2(\tau_b) = \frac{1}{n_b} \sum_{b=1}^{n_b} (\langle u \rangle_b - \langle u \rangle_{run})^2 \tag{A5}$$

where $\langle u \rangle_{run}$ represents the average over the whole run. As τ_b increases, $\sigma^2(\tau_b)$ should become inversely proportional to τ_b, although at the same time n_b will fall, making our estimate of $\sigma^2(\tau_b)$ less reliable. We wish to use this data to estimate $\sigma^2(\tau_{run})$, the variance in the run average. The statistical inefficiency is defined as

$$s = \lim_{\tau_b \to \infty} \frac{\tau_b \sigma^2(\tau_b)}{\sigma^2(1)} \equiv \lim_{\tau_b \to \infty} s(\tau_b) \tag{A6}$$

where the denominator is just the variance $\sigma^2(1) = \sigma^2 = \langle (u - \langle u \rangle_{run})^2 \rangle$ calculated from instantaneous values of u. By plotting $s(\tau_b)$ as a function of τ_b and extrapolating to $\tau_b = \infty$, we can estimate s and hence

$$\sigma^2(\tau_{run}) = s\sigma^2(1)/\tau_{run}. \tag{A7}$$

We have carried out this procedure for all runs of 24 000 sweeps or more for both the configurational energy and the herring-bone order parameter. Typical results are

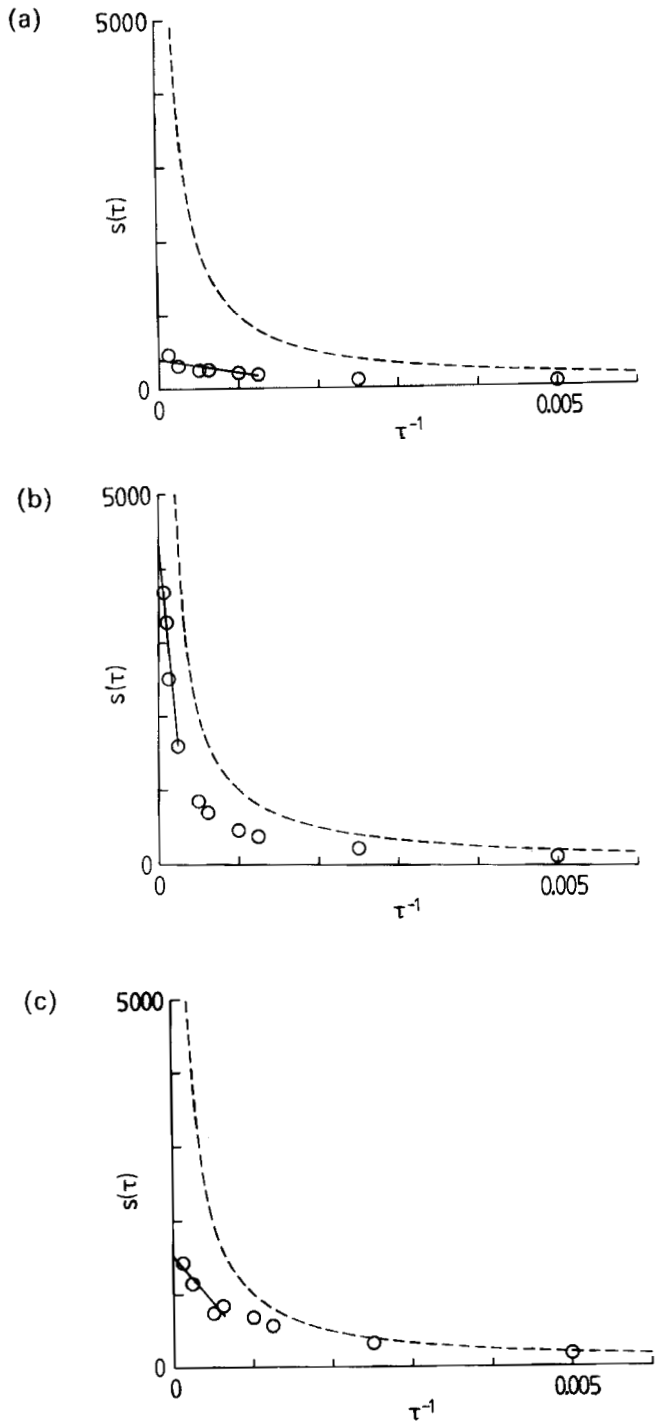

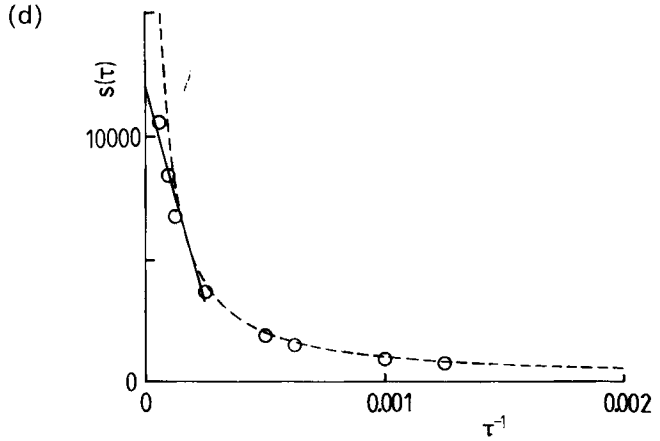

Figure 10 Calculating the statistical inefficiency for the configurational energy u' and the order parameter h. We plot $s(\tau_b)$ vs τ_b^{-1}. In each case, the dashed curve is the limiting low-τ_b hyperbola and the solid line is the linear extrapolation at low τ_b^{-1}. (a) $T = 10.80$ (heating), u'; (b) $T = 11.10$ (cooling), u'; (c) $T = 10.80$ (heating), h; (d) $T = 11.10$ (cooling), h (note change of scales).

shown in Figure 10. On the assumption that s varies smoothly across the range of temperatures examined in this study, with a peak close to the transition, we used these values to estimate error bars for Figure 1 and 2.

It should be noted that we plotted $s(\tau_b)$ vs τ_b^{-1} as originally recommended by Jacucci and Rahman [16] rather than $\tau_b^{1/2}$ as used recently [18]. We prefer our method since it gives a limiting linear plot rather than a plateau value approached algebraically slowly. It is instructive to examine the limiting behaviour from the viewpoint of time averages as measured in molecular dynamics rather than Monte Carlo averages, although a similar analysis applies in the latter case [19]. For a time average, taken over a time t_{av},

$$\langle u \rangle_{t_{av}} = \frac{1}{t_{av}} \int_0^{t_{av}} u(t)dt \tag{A8}$$

the standard result for the variance is related to the correlation function [20]

$$\sigma^2(t_{av}) = \frac{2}{t_{av}} \int_0^{t_{av}} (1 - t/t_{av}) \langle \delta u(0)\delta u(t) \rangle \, dt \tag{A9}$$

where $\delta u = u - \langle u \rangle$. For averaging times much shorter than the correlation time of u, t_u, we have

$$\sigma^2(t_{av} \ll t_u) = \sigma^2 \tag{A10}$$

i.e. the usual variance, independent of the exact value of t_{av}. Averaging over long times gives

$$\begin{aligned} \sigma^2(t_{av} \gg t_u) &= \frac{2}{t_{av}} \int_0^{\infty} \langle \delta u(0)\delta u(t) \rangle dt - \frac{2}{t_{av}^2} \int_0^{\infty} t \langle \delta u(0)\delta u(t) \rangle dt \\ &= \frac{2t_u}{t_{av}} \sigma^2 - \frac{2}{t_{av}^2} \int_0^{\infty} t \langle \delta u(0)\delta u(t) \rangle \, dt \end{aligned} \tag{A11}$$

where we have inserted the definition of the correlation time t_u,

$$t_u = \int_0^\infty \langle \delta u(0) \delta u(t) \rangle dt / \langle \delta u^2 \rangle$$

$$= \int_0^\infty \langle \delta u(0) \delta u(t) \rangle dt / \sigma^2. \qquad \text{(A12)}$$

It is the first term on the right of Equation (A11) that leads to the dominant inverse-t_{av} dependence of $\sigma^2(t_{av})$, and we note that it and the definition (A6) lead to $s = 2t_u$ where t_u is measured in sweeps or timesteps. The second term on the right of Equation (A11) leads us to plot $t_{av}\sigma^2(t_{av})/\sigma^2$ vs t_{av}^{-1} or in our case $\tau_b\sigma^2(\tau_b)/\sigma^2$ vs τ_b^{-1} in order to estimate s. Returning to Figure 10, we expect the data $s(\tau_b)$ to break away from the universal short-time hyperbola implied by Equation (A10) to give a well-defined linear approach to the intercept at $\tau_b^{-1} = 0$. For values away from the transition this is observed, with s for the order parameter being significantly longer than for u', but still well within total simulation run lengths. The extrapolated value of s also acts as a guide to the extent of the region over which linear behaviour can be expected to hold, thus allowing a check for self-consistency. At $T = 11.05$ and $T = 11.10$ the situation is different, with the order parameter data being especially problematic. Deviations from the "short-time" hyperbola only occur at very low τ_b^{-1}, so that only a few points, subject to most uncertainty, can be used for the extrapolation. Our estimated values of s are of order 10 000–15 000, but clearly they could be much larger, and it is even possible that correlations might extend over a number of sweeps of the same order as our simulation run lengths. This analysis gives us a quantitative measure of the difficulties facing a simulation close to this type of phase transition, and the above comments apply *a forteriori* to previous work on this system. Finally, we note that any other method of estimating correlation "times" (such as examining the correlation function of u or h) would be an equally valid route to s.

In fitting the energy and order parameter data, we used a function of the form

$$f(T) = \Delta f \tanh\left(\frac{T - T_c}{\Delta T}\right) + a + b(T - T_c) + c(T - T_c)^2. \qquad \text{(A13)}$$

A standard nonlinear least-squares fitting routine was used [21], with weights obtained from the error analysis described above, and all six parameters Δf, ΔT, T_c, a, b, and c allowed to vary freely without constraints. The above function allows for the possibility of a virtually discontinuous change in $f(T)$ at T_c, with $\Delta T \to 0$, but in fact a smooth fit with $\Delta T \approx 0.1$ resulted in every case (Figures 1 and 2). A more sophisticated underlying polynomial function was not needed over the small range of temperatures treated here, as evidenced by the low values of $|c| \sim 10^{-2}$ which gave best fits, and it was not thought that the data merited the introduction of additional features, such as pronounced asymmetry in the temperature derivative of f around T_c. The quality of the fits obtained may be gauged from the χ^2 values of roughly 0.1 for the configurational energy data and 0.05 for the order parameters.